

Modeling and Evaluation of Robust Whole-Hand Caging Manipulation

Raymond R. Ma^{ID}, Student Member, IEEE, Walter G. Bircher^{ID}, Student Member, IEEE,
and Aaron M. Dollar^{ID}, Senior Member, IEEE

Abstract—Human in-hand dexterity can be highly fluid and unstructured, with multiple phalanxes breaking and re-establishing contact during any given task. In contrast, prevailing research in robotic manipulation has focused on highly structured well-controlled motions, where contact points are carefully characterized. Maintaining grasp stability by satisfying traditional closure conditions during complex within-hand manipulation motions can be difficult, even with highly articulated end effectors. However, simple grippers can still achieve an effective range of in-hand manipulation tasks without strict closure conditions, as long as the object can be bounded locally relative to the hand frame. The end effector can be considered as a tool to limit the range of possible object poses. In particular, the energy of the hand-object system can be used to determine an attractor region toward which the hand drives the object. This can be combined with a sparse sampling of the configuration space to find a set of manipulation primitives that can reliably constrain the object inside the hand workspace even without feedback, a strategy proposed as *whole-hand caging manipulation*. In this paper, experimental results with a planar underactuated gripper are presented to validate this manipulation strategy, and it is shown that even though contacts are regularly broken and reformed, the object can be reliably manipulated within the hand workspace without ejection, and challenging movements such as sliding and gaiting can be reliably performed.

Index Terms—Caging, dexterous manipulation, open loop, whole-hand manipulation.

NOMENCLATURE

q	Particular configuration for either object ($q_{obj} \in SE(2)$ or $SE(3)$) or hand ($q_{hand} \in R^N$).
C	Configuration space (C-space) for the object.
C_i	C-obstacle due to the hand's i th component, or the set of object configurations such that it would intersect with the hand's i th component.
H	Configuration space for the hand.

Manuscript received July 19, 2018; accepted November 28, 2018. This paper was recommended for publication by Associate Editor S. Hirai and Editor A. Billard upon evaluation of the reviewers' comments. This work was supported by the National Science Foundation under Grants IIS-1317976 and IIS-0952856. (Corresponding author: Walter G. Bircher.)

R. R. Ma is with the NASA Jet Propulsion Laboratory, Pasadena, CA 91109 USA (e-mail: raymond.r.ma@jpl.nasa.gov).

W. G. Bircher and A. M. Dollar are with the Department of Mechanical Engineering and Materials Science, Yale University, New Haven, CT 06511 USA (e-mail: walter.bircher@yale.edu; aaron.dollar@yale.edu).

Color versions of one or more of the figures in this paper are available online at <http://ieeexplore.ieee.org>.

Digital Object Identifier 10.1109/TRO.2019.2890990

A_{obj}	Region of the object in real space.
A_i	Region of the hand's i th component in real space.
N	Mobility of the hand, number of parameters needed to fully define the hand configuration.
M	Number of discrete components in the hand mechanism, not necessarily equivalent to N .

I. INTRODUCTION

DEXTEROUS manipulation is regularly described as a skillful use of the end effector to arbitrarily adjust the object pose relative to the hand frame, in order to augment the capabilities of the manipulator arm [1]. For example, this may be done for fine positioning of the object in pick-and-place tasks, or to regrasp the object such that it is secured or exposed more optimally for some operation. Traditionally, in-hand manipulation has been modeled as a set of independently controlled fingers applying some controlled load, or wrench, to the object through a set of point contacts. The fingers, usually represented as fully actuated serial chains, are coordinated such that the desired stability and closure conditions are maintained as the system modulates the object pose [2], [3]. Despite extensive study in this area, physical implementations of dexterity with robotic hands have remained a major challenge, even with recent advances in hardware [4] and control fidelity [5], due to the high degree of complexity that this approach requires.

However, in-hand dexterity is not necessarily restricted to manipulation with fingertips exclusively [6], nor do hands need to always maintain closure conditions throughout the commanded task [7]. Consider the task of picking a screwdriver out of a cluttered bin and reorienting it properly into a secure grip for use. As the screwdriver is transitioned into the desired grasp, the number and location of contacts may change frequently, and there are likely many transitional instances where even a small external wrench would be enough to eject the tool from the hand. However, it can be argued that the task is considered successful as long as the screwdriver can eventually be secured into the desired grasp. We propose that the manner in which the object reaches the target pose or how the contact conditions change, disengage, and re-establish is not critical. By relaxing some of the constraints and requirements in traditional manipulation, other useful and simpler control strategies can be explored. As shown in Fig. 1, very simple motions can produce in-hand dexterity, without needing to characterize the specifics of the overall system to keep the object securely fixed to the hand.

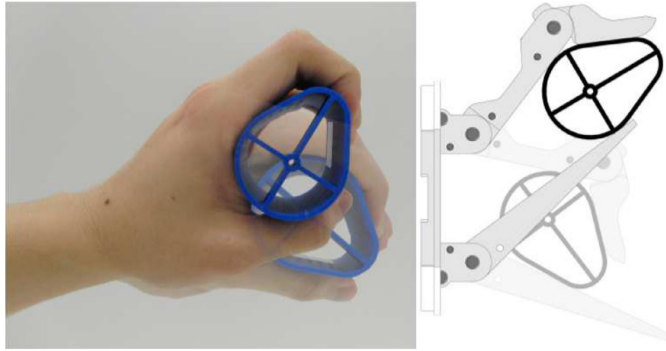


Fig. 1. Examples of in-hand manipulation via caging and whole-hand grasping as shown by both anthropomorphic and robotic systems.

Caging has been proposed as a robust method to bound the permissible range of poses for an object in the context of mobile, distributed robotics in the plane [8], and also for robotic grasping and manipulation [19], [20]. This approach simplifies the control scheme by permitting a limited amount of object free motion, recognizing that the system does not need to fully constrain the object during every phase of the task. Researchers have recently begun to acknowledge the potential utility for robotic hands performing caging primitives [9]–[12], [37]–[39], but to our knowledge, none have modeled or evaluated the repeatability of this strategy for in-hand manipulation with physical robotic grippers.

In a similar manner, underactuated adaptive grasping has been validated as a reliable method of fixturing an object to the hand, without requiring coordinated control, *a priori* knowledge of object geometry, or tracking of contact conditions. This “let the fingers fall where they may” approach [13], [14] uses the same control input to reliably engage and maintain secure contact with a range of object shapes. Even though not all degrees of freedom in the system are controllable, mechanical design parameters and control strategies can be tuned to generate a repeatable set of behaviors that are guaranteed to stay within acceptable bounds [15].

In this paper, we detail the concept of whole-hand manipulation via caging, or *caging manipulation*, a dexterous control strategy especially well-suited for simple and/or underactuated grippers [34]. This control methodology only requires the object to start within a local *capture region* [16] in the hand workspace, not any particular precision or power-grasp configurations, and it does not require any coordination between contact points. Even simple hands with a limited number of actuators can be configured such that even in the absence of force or form closure conditions, the object configuration space can be adequately limited and localized. This approach allows for robust open-loop control and can be shown to produce highly repeatable results without needing to characterize or track the contact conditions. Passive grasp adaptability through underactuated design can then be leveraged to further constrain the object after manipulation completes. An object-centric energy model adapted from relevant past work [13], [17] is used to analyze the expected behavior of the hand-object system. Extensive experimental results from the implementation of a planar underactuated hand

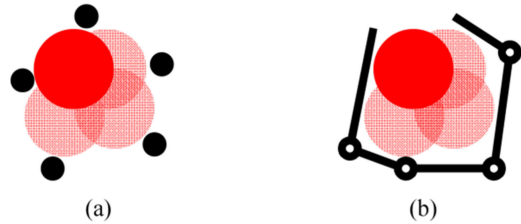


Fig. 2. Manipulated object (shown in red) can be caged via point obstacles (a) or hand/gripper components (b).

and several object geometries will be presented to demonstrate the efficacy of this approach, and the effects of friction as well as the viability of gaiting motions will be discussed.

II. CAGING MANIPULATION MODEL

The manipulation strategy and model described in this paper combines previous work done on caging with linkage-based grippers [9], [10] and energy-based evaluation of underactuated hands’ ability to hold and localize [13], [17].

An ideal unconstrained object alone can be freely moved in its configuration space without any additional energy. Obstacles that are introduced into the object configuration space reduce its free workspace, and a hand can be thought of as a collection of rigid and compliant obstacles relative to the object. Unlike the traditional notion of caging, which assumes static obstacles that generate inaccessible regions in the object workspace, we recognize that actuated components, such as finger phalanges and gripper surfaces, have an associated energy state [13], [17] such that a sufficient force applied externally to the object can displace these components. It can be assumed that work must be done on a caging hand configuration to reconfigure it into a noncaging configuration that can allow the object to escape.

The reciprocal system characteristic is also true: In the absence of an object or other components, an actuated component in a conservative system should resolve to the lowest possible energy state. Similar to how a caging structure limits the object mobility within a finite subset of possible configurations, an object within a grasp limits the range of possible hand poses. For example, a finger actuated with a constant torque input will attempt to close fully, until it contacts an obstacle that restricts its motion or reaches a physical hard stop. In this way, we extend caging beyond a purely kinematic analysis by accounting for reconfigurations in the hand-object system and their relative energy states.

A. Traditional Caging Formulation

In summary, an object is caged if it cannot be moved to a point at infinity without intersecting other components in its workspace. Fig. 2 compares the traditional caging problem, commonly utilizing point-based obstacles, and the corresponding caging problem for a planar two-finger hand, which can be represented by a set of serial chains. Traditionally, the caging manipulation model is a purely geometric evaluation that uses the nomenclature, extended from [10] for consistency.

The set of allowable nonintersecting hand configurations H_{free} is first determined by the constraint

$$H_{\text{free}} := \left\{ q_{\text{hand}} \in H \mid \bigcup_{i=1}^{M-1} \bigcup_{j=i+1}^M A_i(q_{\text{hand}}) \cap A_j(q_{\text{hand}}) = \emptyset \right\} \quad (1)$$

where no hand component intersects, or occupies the same real space, as any other component of the hand. For simplicity, relevant work typically assumes point or line-based obstacles, or simple geometries that can be decomposed into those primitives.

For a given hand configuration, each hand component obstructs a subset of the object's configuration space

$$C_i(q_{\text{hand}}) := \{q_{\text{obj}} \in C \mid A_{\text{obj}}(q_{\text{obj}}) \cap A_i(q_{\text{hand}}) \neq \emptyset\}. \quad (2)$$

The combined set of restrictions in the object configuration space due to the hand is then

$$C_{\text{hand}}(q_{\text{hand}}) := \bigcup_{i=1}^M C_i(q_{\text{hand}}). \quad (3)$$

Consequently, the object configuration space when accounting for the hand as an obstacle is

$$C_{\text{obj}} = C \setminus C_{\text{hand}}. \quad (4)$$

Caging is defined when C_{obj} can be separated into two disjoint nonempty sets: C_{Inf} , which contains a point at infinity, and C_{cage} , the configuration subspace that is surrounded by C_{hand} . There is no path from any point in C_{cage} to infinity that does not go through C_{hand} . In other words

$$C = C_{\text{cage}} \cup C_{\text{inf}} \cup C_{\text{hand}} \quad (5)$$

$$C_{\text{cage}} \neq \emptyset \quad (6)$$

$$C_{\text{cage}} \cap C_{\text{inf}} = \emptyset. \quad (7)$$

B. Energy Model for Manipulation Capability

As in form closure, the conventional definition of caging assumes rigid immovable C obstacles. However, actuators may not necessarily reach their commanded reference poses due to geometric constraints in the system. Physical systems do not have ideal actuators, so they cannot resist arbitrarily large external forces or torques. In fact, several researchers [17], [18] have emphasized the importance of evaluating the effect of pull-out forces for various grasp configurations in design implementations, because the final system state is determined by the interactions between a number of active and passive elements in the system.

Furthermore, while previous work [19], [20], [36] have considered the application of conventional caging to manipulation, a purely geometric approach cannot account for how contact interactions may reconfigure the hand-object system. For stable in-hand manipulation tasks, it may not be sufficient or possible to only bound the object's caged configuration space C_{cage} , even if it is limited to a single pose in the case of form closure. A hand generally applies forces at contact to the object, and especially in the case of underactuated mechanisms, the stable system configuration and resultant applied forces are coupled,

not independently controlled [15], [21]. It is, therefore, useful to not only focus analysis on caging configurations that minimize C_{cage} , but also consider grasps as a set of reconfigurable cages.

Assuming a conservative system with no dissipative elements, a stable grasp configuration for a given set of actuation inputs is represented by an energy minimum configuration. Energy minimization has been an especially useful analytical tool to determine how underactuated mechanisms reconfigure. Prior models for underactuated in-hand manipulation only considered consistent contact conditions, usually either point or rolling contacts with no slip [2], [15], [22]. A more comprehensive energy gradient field, composed of the calculated energies from the full set of system configurations for various contact conditions, provides insight into not only how the system behaves under the influence of external forces, but also how the system reaches an energy minimum configuration.

Instead of considering only rigid caging configurations, we propose the concept of a *manipulable cage*, caging configurations that can be reconfigured into other caging or noncaging configurations with some nonzero work. Relative to the commanded reference inputs, the work done by the actuators can be mapped to the corresponding object configuration satisfying the contact constraints of the manipulator [17]. Mahler *et al.* [23], [35] have presented a similar concept called *energy-bounded caging*, configurations which effectively cage the object with the assistance of some external force, such as gravity. In both of these definitions, an escape path in the energy field can be computed for a caged object, and the energy expenditure necessary to free the object is calculated.

This model utilizes a simple position-based control for each actuator. The most basic actuators typically exhibit some compliance margin around the goal position where the actuation torque or force is proportional to the error. Outside of this margin, the actuator saturates to a constant torque or force output. For simplicity, we assume bang–bang control such that the actuation energy for a given reference value a_k , either position p_A (for linear actuators) or rotation θ_A (for rotary actuators), for the k th actuated component is

$$E_{Ak}(p_k) = -f_{Ak}(p_k - p_{Ak}) \quad (8)$$

$$E_{Ak}(\theta_k) = -\tau_{Ak}(\theta_k - \theta_{Ak}) = -f_{Ak}r_{Ak}(\theta_k - \theta_{Ak}) \quad (9)$$

for actuation force f_A , or actuation torque τ_A and corresponding transmission radius r_A . In the context of hands, we also assume in this paper that actuated components (most commonly tendon-driven finger phalanges) can only push, not pull, so configurations with negative energy values, indicating configurations where the actuator can achieve the reference input without the associated actuated components making contact with the object, are treated as zero-energy configurations. Also, as this energy value is only a relative measure, the reference position is bound by the object-contact space's limitations on the actuator workspace.

Manipulator components may also have passive elements, like return springs or flexural stiffness in underactuated hand designs [14], [17], contributing an energy component $E_P(q, K, q_0)$ determined by the configuration q , stiffness

matrix K accounting for the spring constants, and rest configuration q_0 . However, it can be argued that, in practice, active actuation forces should be significantly larger than passive forces; therefore, we do not take them into account in the present formulation. We also do not consider the potential energy component due to gravity in this paper, since the plane of manipulation is assumed to be at a constant height.

The full system energy for each configuration is then the summation of the energy for all actuators

$$E_A(a_{\text{hand}}) = \sum_k^N \max(E_{Ak}(a_k), 0). \quad (10)$$

Under the assumptions of this model, each actuator is at its lowest energy configuration at the target commanded reference. For example, actuated components at the given reference value have an energy of 0, but its energy state increases as it is displaced from that reference configuration. In a multicomponent system, interactions and interferences between components can make it impossible for each actuator to achieve its commanded reference. The system is expected to reconfigure toward the lowest energy configuration of all the possible system configurations permitted by the components' geometries and respective workspaces.

The goal of the manipulation analysis detailed in this paper is to generate a potential field with respect to the hand-object configuration space for each set of actuation inputs in order to determine the expected object behavior under different caging or grasp conditions. For each unique object pose $q_{\text{obj}} (\in SE(2)\text{or }SE(3))$ within its configuration space, the system energy is calculated for all valid hand configurations q_{hand} that do not intersect the object geometry, and the minimum-energy hand configuration for this subset is recorded. The object-hand energy field is then the set of all object poses corresponding to valid minimum-energy hand configurations.

The calculated energy field for the caged object summarizes its expected response to each applied hand input, not just the characteristics of an individual object pose. As detailed in past literature [7], [24], [25], a grasp is considered stable, though not necessarily in form or force closure, if there exists a potential function V such that any disturbance twist or displacement from the equilibrium configuration creates a restoring force and increases the potential energy of the system. Likewise, the energy gradient is zero and the corresponding Hessian matrix is expected to be positive definite at stable grasp configurations. The magnitude of the energy gradients local to any point in the object configuration space correspond to the net force magnitudes acting on the object. In this way, each caging manipulation primitive establishes a particular region of attraction in the object workspace. These details can be numerically extracted from the object energy field to provide more insight regarding the grasp stiffness and the effective bias that the hand applies to the object pose [25].

It should be emphasized that the analysis presented here only characterizes the object behavior with respect to some hand system and a set of inputs. This model does not necessarily guarantee a global energy minimum, reachability of all caging

TABLE I
OBJECT ENERGY FIELD METHODOLOGY PSEUDOCODE

```

For each hand configuration  $q_{\text{hand}}$ :
  If  $\text{isCaging}(q_{\text{hand}})$ ,  $S_{\text{caging}} \leftarrow q_{\text{hand}}$ 
For each caging hand configuration  $q_{\text{caging}} \in S_{\text{caging}}$ 
  For each actuated component  $AC_j$ :
    Calculate object contact subspace  $CS_j(q_{\text{caging}})$ 
    Add  $\cap_j^p CS_j(q_{\text{caging}}), q_{\text{caging}}$  to object contact space
     $OC$ 
  For each  $q_{\text{obj}}, q_{\text{caging}} \in OC$ :
    Calculate  $E_A(q_{\text{caging}})$ 
    Add  $q_{\text{obj}}, \min(E_A(q_{\text{caging}}), EO(q_{\text{obj}}))$  to object energy
    field  $EO$ 

```

configurations, or sustained contact and object stability between energy minimal configurations. The simple hand models and object geometries utilized in this paper avoid those degenerate cases, but future work will need to address limitations of the energy minimal approach, especially for use in manipulation and grasping planners.

III. OBJECT ENERGY FIELD METHODOLOGY

It is computationally prohibitive to sample all possible hand configurations for each object pose, so observations about whole-hand manipulation with traditional grippers were leveraged to minimize the computational complexity of calculating the energy field. First, the presented analysis only considers convex object geometries (or the convex hull of evaluated objects) and ignores cases where hand features may form caging configurations via concave features on the object. Next, only a small subset of the hand's configuration space includes valid caging configurations, so the noncaging configurations that cannot constrain the object are disregarded in the analysis. Also, as we are interested in manipulation, not just containment, we can prioritize configurations where all actuators are actively driving a component, or set of components, that makes contact with the object. Consequently, instead of sampling all possible hand configurations for the entire object configuration space, it can be sufficient to focus on the *caged object-contact space*, the set of object-hand configurations where the hand cages the object and work is being done on all actuators due to object contact. The implemented methodology is summarized in Table I.

A. Planar Caging Condition

For efficiency, this methodology first calculates all possible caging configurations for a hand design, irrespective of the target object, as shown in Fig. 3. In the planar case, this caging problem can be simplified to two sub-problems regarding the grasp polygon: finding the minimum opening length L_{Open} and the diameter of the maximal inscribed circle L_{Obj} , as detailed in Fig. 3. The *grasp polygon* is the planar polygon with edges formed by the finger phalanges, the palm surface, and the edge between the pair of distal fingertips. For the common case with two opposition fingers, the minimal opening can be found as either the magnitude of the vector between the distal fingertips

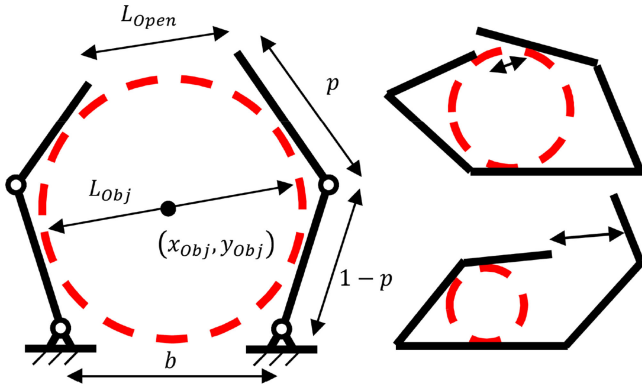


Fig. 3. Caging capability of a planar hand configuration can be efficiently approximated by the largest inscribed circle with diameter L_{obj} and the smallest escape opening length L_{open} of the grasp polygon: The region bounded by the hand components.

or the vector between a distal fingertip and an opposing phalanx, perpendicular to that phalanx. The maximal inscribed circle is found by iterating through all unique triplets of grasp polygon edges and finding the circles tangent to all three edges with centers lying within the grasp polygon.

The planar gripper shown in Fig. 3 forms the basis for the simulation and experimental work presented in this paper, and its design can be reduced to the primary parameters p and b . The authors' previous work [7], [21] utilized normalized design parameters $b = 0.6$ and $p = 0.37$ for both fingers, a design denoted as the Model T42. This paper also evaluated variations to the base design: a shorter proximal linkage in one of the fingers (T42a), and a one-link finger (or thumb) in place of the standard two-link finger (T42b). Fig. 4 details these design variations further.

B. Object-Contact Space

Each object can be designated by the set of points $p_1 \dots p_Q \in P_{\text{obj}}$ in its convex hull, relative to some arbitrary object center p_o . The hand mechanism can be simplified as a set of serial chains with zero thickness. A constant finger thickness in the physical system can be accounted for by adding an equivalent padding to the object geometry in this simulation.

In this simplified scenario, the object-contact space relative to a single link can be found for each object orientation by taking the pair of link endpoints $S_i = (s_{i1}, s_{i2})$ for link L_i , relative to the hand frame, and first computing the Minkowski sum $MS_i = S_i \oplus (-P_{\text{obj}})$. This gives the set of all object positions where at least one point on the object boundary is coincident with a link endpoint. Then, the subset of these object center points where all the corresponding object boundary points are on the same side of the finger link, such that no part of the object intersects the finger geometry in that configuration, can be found by finding the convex hull CH_i of the points in MS_i . The object-contact space CL_i relative to a single link is finalized by interpolating between adjacent points in CH_i . In this paper, interpolation guaranteed a nearest neighbor distance of 0.02 normalized with respect to the total representative finger length. For multilink fingers, the object-contact space CL_i of each link

should also exclude points that are within the convex hulls of other links in the same serial chain. The contact space CS_j for the entire serial-chain finger of B links is then the union of the final contact spaces for each individual link, $\bigcup_{i=1}^B CL_i$.

The object-contact space for the entire mechanism is the intersection of the contact spaces $\bigcap_{j=1}^P CS_j$ calculated for the actuated components of interest. For the planar underactuated hand designs investigated in this paper, that space is comprised of configurations where the object makes contact with both fingers. While it is possible for the hand to immobilize the object with only a single finger, those configurations are not particularly meaningful for manipulation. Also, by utilizing the contact spaces for each finger as opposed to each link separately, this approach accounts for both cases where the object makes contact with a single finger link or both. For more complex hands, especially ones where not all actuated components necessarily need to contact the object during manipulation, the different permutations of actuated components would need to be considered.

To calculate the intersection, it is sufficient to find pairs of points where the pairwise distance is less than the discretization used to formulate the contact space. For computational efficiency, we generated a discretized Cartesian grid for the object workspace with spacing 1 mm, and in the planar, two-finger case, contact with both fingers was assumed when a point from the object-contact spaces of both fingers occupied the same grid cell.

The method described here was repeated for all object orientations and sampled hand configurations to calculate the overall object-contact space OC , the set of all object configurations q_{obj} with a corresponding caging configuration q_{caging} that ensures contact between the object and each actuated finger. This sampled subspace accounts for all the ways that the hand can reconfigure while maintaining some form of contact, and consequently interacting, with the object.

C. Object Energy Field

With the full contact space calculated, the system energy can be calculated directly with respect to each valid hand-object configuration, as described in Section III-B, to complete the formulation of the energy field, for a given set of actuation inputs. Since the methodology presented here uses the same object-contact space for all actuation inputs, it is straightforward to evaluate the full actuation workspace. In other words, the energy state is dependent not only on the hand configuration, but also on the object geometry, which determines the set of hand configurations that should be considered. Note that for underactuated actuation schemes, the entire finger, rather than individual phalanges, serves as the actuated component.

For each set of actuation inputs, we can also segment the object energy field based on whether all actuated components make some form of contact with the object by identifying the configurations where the energy values for all independent actuated components are nonnegative. Keep in mind that the object energy field for a particular set of actuation inputs can denote a nonnegative energy value without all fingers making contact with the object. As an example, fingers can be actuated such that

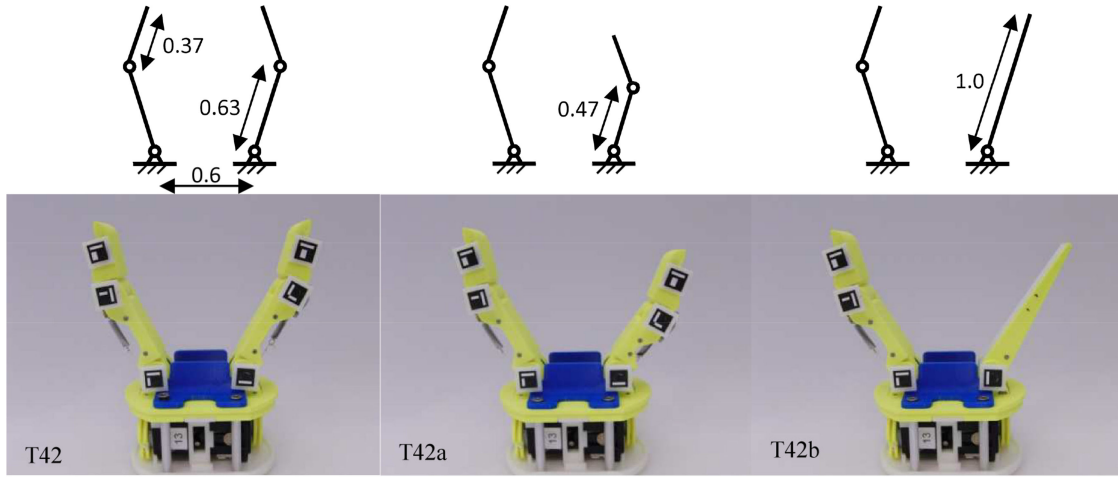


Fig. 4. Three different manipulators (T42, T42a, and T42b) that were evaluated in this paper for a variety of object geometries. The physical implementation utilized fingers of total length 100 mm.

the actuators reach the target reference input while only loosely caging the object. In this case, there would still be nonnegative energy values for object configurations where the object does work against at least one of the fingers, but never both.

D. Case Study—Model T42b

Consider the manipulation of a planar object with the T42b, the hand design variation with an underactuated two-link finger on the left, and an opposing, one-link thumb. For an arbitrarily selected actuation input [0.4, 0.7] applied to the T42b, Fig. 5 shows the xy object energy fields for a square object at various orientation values. The energy values are normalized with respect to the maximum energy configuration across all orientations. Note that the xy contact space changes for different θ values, and this particular control input drives the object toward a pose with one of the square edges aligned with the base of the hand ($\theta = n\pi/2$). For this case study, the underactuated finger utilized an actuation ratio of 1.0 such that the proximal and distal joint torques are equivalent. Alternative actuation ratios would cause the two-link finger to reconfigure differently, resulting in a different energy field distribution for the same contact object space.

As shown in Fig. 5 (and later in Fig. 6), the object energy field can be plotted for a range of actuation inputs $[a_1, a_2]$, where a_1 and a_2 drive the one-link thumb and two-link finger, respectively, to more extensively profile the hand's manipulation capabilities. The energy field analysis shows that the object is pulled inward and resists ejection from the hand workspace due to the caging configurations. Relative to the overall object-contact space, the range of minimal-energy object configurations for the full actuation workspace is limited, indicative of the additional robustness of a caging, power grasp in comparison to a force-closure precision grasp with point contacts.

In particular, consider the example in Fig. 6 with actuation inputs [0.4, 0.4] in the lower left. Even though there is no object-hand configuration such that both fingers make contact with the object while doing work, energy is still required to move the

object from the innermost energy-minimal region to outside of the object-contact space. Work must be done against at least one of the fingers in order to eject the object.

IV. EXPERIMENTAL PROCEDURE

To evaluate this manipulation strategy experimentally, we explored the planar caging-manipulation workspace and manipulation trajectories for various object geometries [see Fig. 7(a)]. Aside from the basic circle, rectangle, and square geometries, a range of egg geometries, determined by a 25-mm diameter circle and a 45-mm diameter circle with a variable offset between the two, were evaluated. All objects were printed and had attachment points for fiducial markers. All tested hands, as shown in Fig. 4, were tendon driven with revolute joints and used the same actuation base, with two Dynamixel RX-28 smart servos, each independently driving a finger. To minimize friction, the urethane fingerpads usually implemented in the designs were removed. Both the finger and object surfaces were Acrylonitrile butadiene styrene (ABS) three-dimensional printed with layers oriented in the same direction.

A. Physical Test Setup

Fig. 7(b) summarizes the physical experimental setup used to assess the hands' caging-manipulation capabilities. A Logitech C920 webcam was mounted above the test hand, which was fixtured in place. Aruco fiducial markers [26] were affixed to the test object centroid and ends of each finger link, via the revolute joint center where possible. Using Python and OpenCV for image capture and fiducial tracking, this setup could record at approximately 15 frames/s. For each commanded actuation input, the marker positions were tracked and recorded continuously throughout the motion, but the actuator positions were only recorded at the start and end of each motion, due to Dynamixel servo latency. The mapping between the camera and real-world coordinates and the hand reference frame were extracted from the marker locations for the proximal joints, which should be static for all tests.

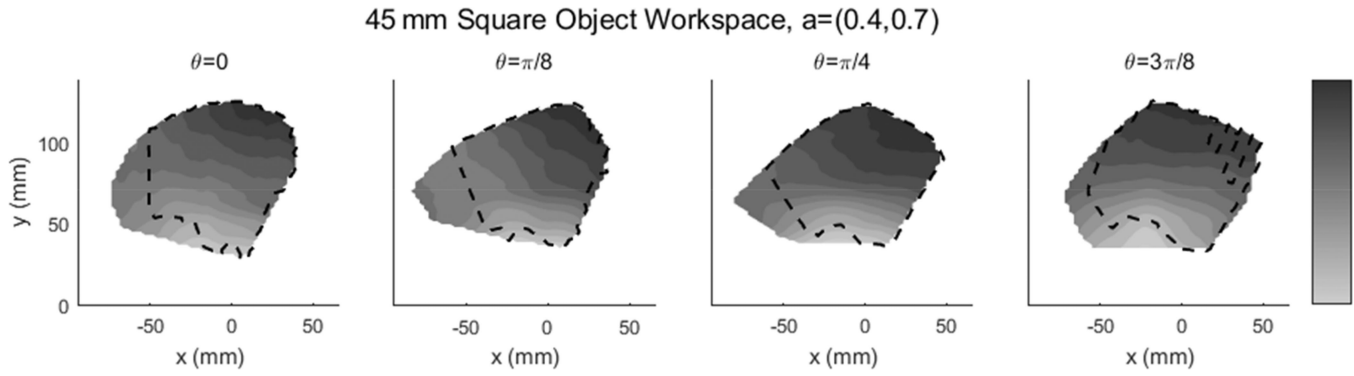


Fig. 5. Energy field plots for a range of object orientations in the simulated evaluation of the T42b hand and a square object for fixed actuation input [0.4, 0.7]. The energy fields vary for different object orientations due to different contact spaces. The dotted outline designates the bounds of the object's contact space where the object is in contact with and doing positive work on both fingers (the dotted line enclosing empty space for the $\theta = 3\pi/8$ case is due to an approximation error in calculating the bounds).

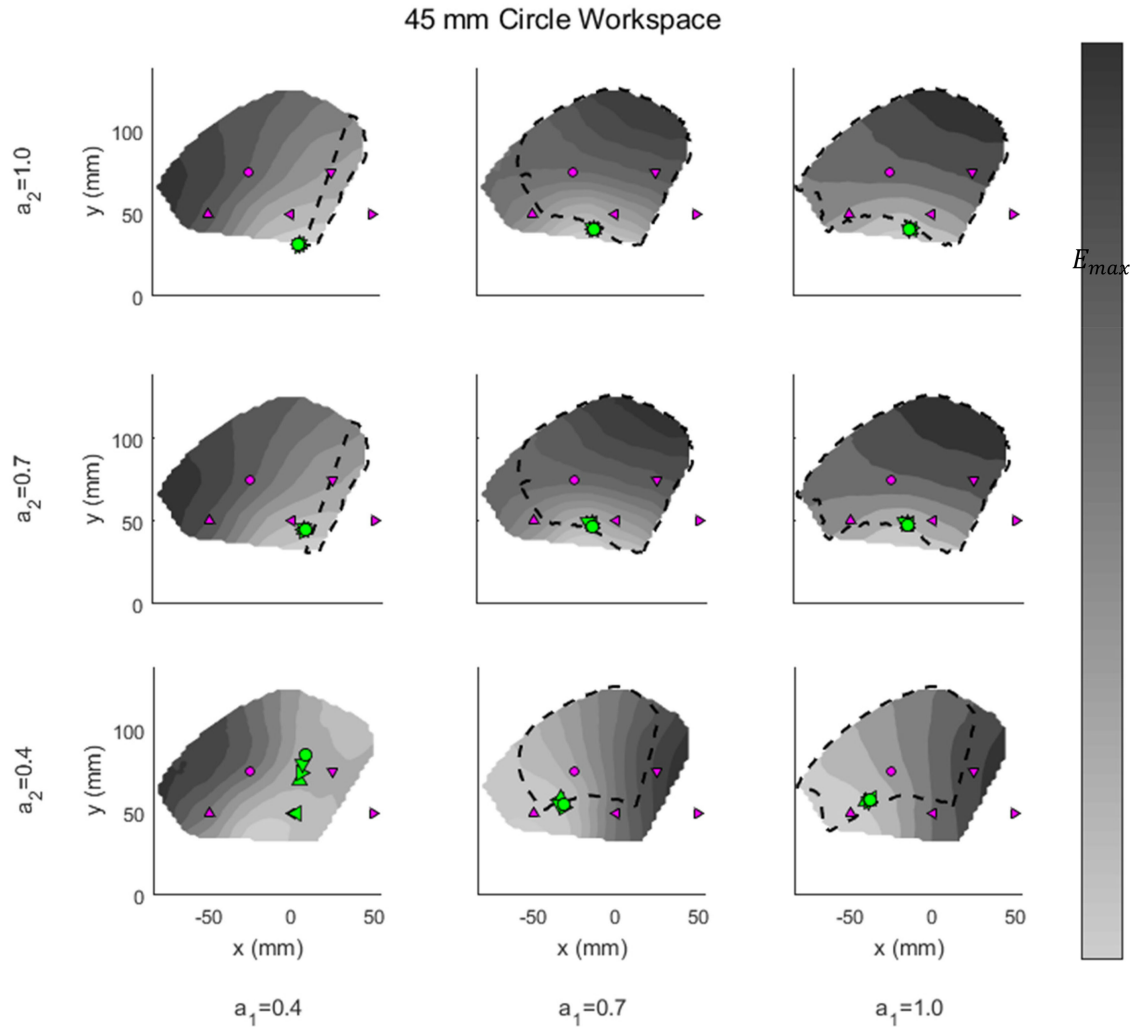


Fig. 6. 3×3 grid of simulated object energy fields for the T42b hand and a circular object. The energy values for each actuation input are normalized with respect to the maximum energy configuration in that particular input pair. Symbols represent experimental object start points (small symbols) and end points (large symbols). For example, the object moves from small circle to large circle after the hand is commanded with the corresponding actuation input. The objects tend to come to rest with both fingers in contact (inside the dotted lines), once they reach the edge of the relatively flat low energy regions.

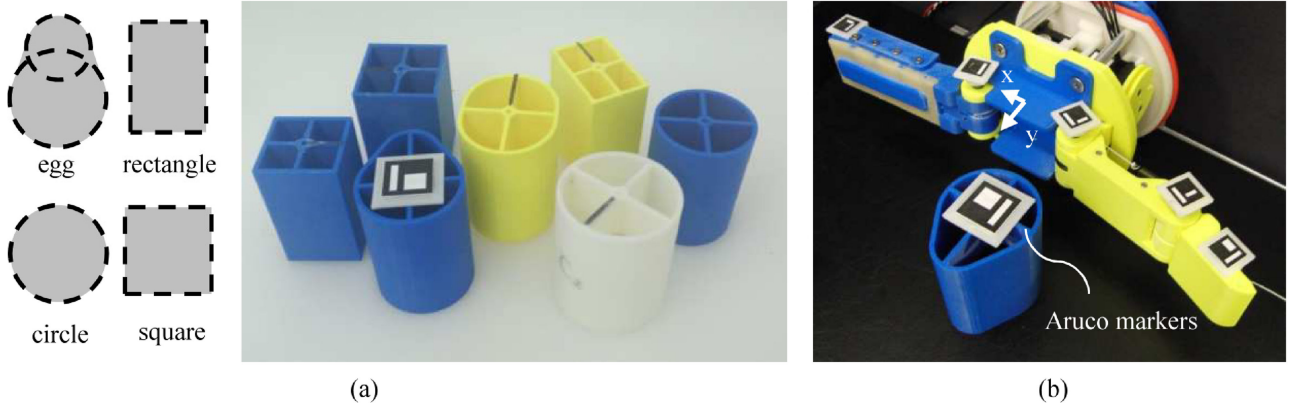


Fig. 7. (a) Various object geometries evaluated by the proposed caging manipulation experimental study. (b) Experimental setup with Aruco markers used in this paper. A webcam was mounted above this setup to record object and finger motion.

B. Actuation Space Exploration

To generate the viable actuation space for each object, we took advantage of underactuated hands' mechanical adaptability. Each actuator's operating range was first discretized, and for each actuator, it was driven to each discretized value via position control. The other actuators were then commanded to close via a constant torque, and the actuator encoder values were recorded after the object and hand elements were fully constrained in a stable grasp, if possible. This exploration excluded cases where the hand ejected the object during grasp acquisition or where the hand configuration was visually identified as a noncaging. The object was reset to the middle of the hand workspace between each grasp acquisition test. This sparse sampling of points in the actuator space was then interpolated to produce the set of actuator inputs used in the workspace evaluation.

C. Object Workspace Exploration

With any given actuation space, the exploration procedure iterated through and tested all possible initial and target combinations of actuator inputs. In order to account for contact variability and/or hysteresis in the pulley transmission, the actuators are initially driven to their target values in position mode, and then switched to torque mode to maximize contact. The actuator encoder positions were only recorded after motion of all hand components resolved, and the object-hand system was immobile. Fig. 8 summarizes these steps in a typical tested manipulation execution.

Unlike past work studying in-hand manipulation with underactuated hands [27], which required the object to be reset into a stable pinch grasp between each manipulation attempt, the actuations inputs calculated in the previous section are sufficient to keep the object within the grasp acquisition range and avoiding ejection. As a result, each workspace exploration could be run continuously. A typical exploration of the full actuation space evaluates ~ 160 independent motion trajectories, lasting a total duration of 20 min. At least two full workspace exploration trials were completed for each unique hand-object combination.

A hybrid k -nearest-neighbors (KNN) approach was used to remove outliers from the experimental data. A similar approach

is implemented in the point cloud library [28]. For each point p_i in set P , the algorithm calculates the distances to the KNN, D_i , where $k = \sqrt{n}$, and n is the size of the dataset. The maximum such distance for each point, $\max(D_i)$, was recorded in set D_{\max} , and points p_i with $\max(D_i)$ outside the range $\text{mean}(D_{\max}) \pm 1.96 \text{ std}(D_{\max})$ were removed. This algorithm is independent of coordinate-frame selection, does not bias the resulting workspace toward any shape or convexity, and still performs well for sparse datasets.

D. Trajectory Test Cases

Experiments were performed to assess how well object motion followed simulated energy gradients, and to observe whether or not objects settled into low-energy positions as predicted by the simulated actuated workspaces. For each actuation input pair, the object was physically placed in five positions in front of the open hand. Then, the hand's motor positions were commanded to an actuation input pair and the object's end point or trajectory was recorded. In the cases where full trajectories were recorded, the servo velocities were slowed so that no frames were lost during the fiducial tracking.

V. EXPERIMENTAL RESULTS

A. Manipulation Workspaces

Examples of the full object workspaces achievable through the proposed caging manipulation are shown in Figs. 9 and 10. The black points designate the final object grasp poses, each independently evaluated via the sequence described in Section IV-B, and the gray points correspond to all object poses during the execution of each caging manipulation move. The results for all the evaluated hand-object combinations are detailed further in Table II. The achievable object workspaces ranged from 13 to 46 mm in the x -direction, 4 to 26 mm in the y -direction, and up to 1.8 rad in total reorientation. As has been previously proposed in past works [17], [18], [27], the manipulation capability is determined by a combination of the hand's geometric design parameters and the object shape.

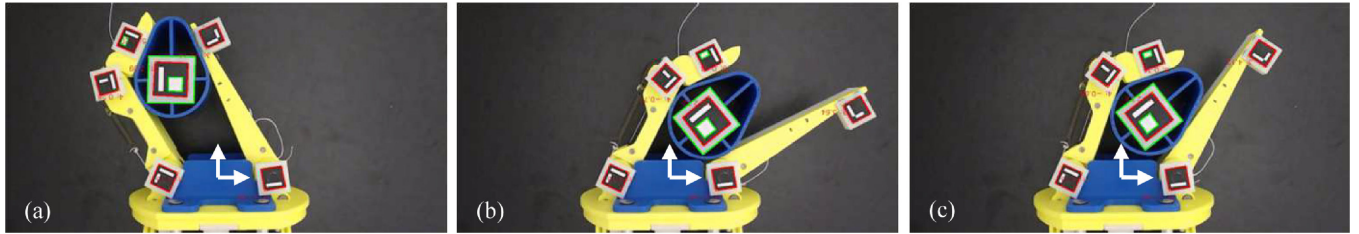


Fig. 8. Summary of an evaluated motion trajectory: From an initial point in actuation space (a), the hand is commanded to the target point in actuation space (b), and after the motion concludes, an open-loop torque-based squeezing operation is commanded to ensure contact.

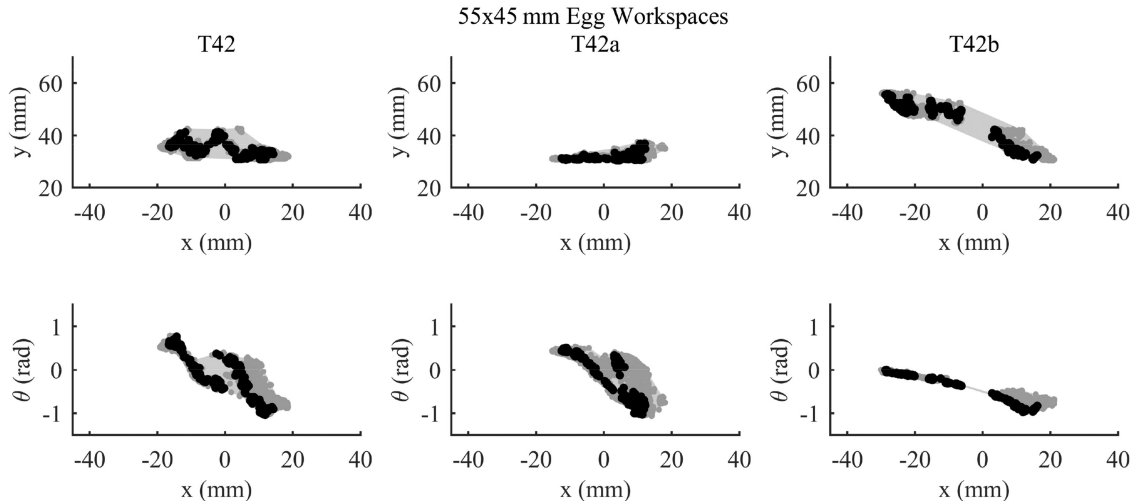


Fig. 9. Experimental workspace results evaluated for a 55×45 mm egg object and the various planar hand designs.

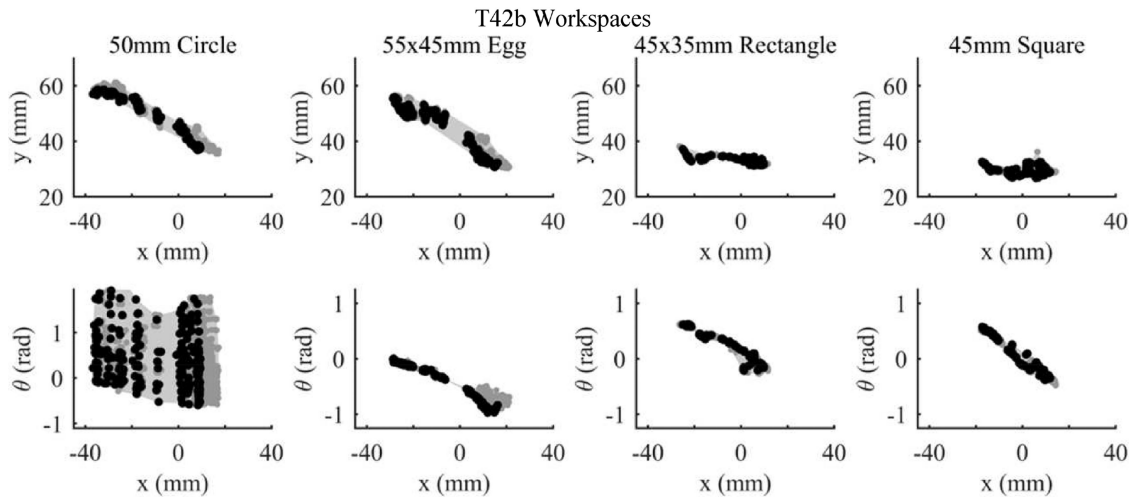


Fig. 10. Experimental workspace results evaluated for the T42b and a set of different object geometries.

1) Effect of Hand Topology: Fig. 9 provides an overview of the variation in object workspace shape for the three-hand design configurations. The T42 produced the most symmetric object workspace with respect to the hand frame. Reducing one of the proximal finger link lengths in the T42a design decreased the achievable workspace. Implementation of the one-link

finger in the T42b increased the workspace range in xy by consistently constraining the object against the distal link of the opposition two-link underactuated finger. The reduced degrees of freedom in the T42b, compared to the T42 and T42a would have been detrimental in the execution of fingertip-based in-hand manipulation [21], but for whole-hand manipulation,

TABLE II
CAGING MANIPULATION EVALUATION—OBJECTS AND HAND DESIGNS

Object	Hand type	$r_s(a_1, x)$	$r_s(a_1, \theta)$	$r_s(a_2, x)$	$r_s(a_2, \theta)$	$range(x)$ (mm)	$range(y)$ (mm)	$range(\theta)$ (rad)
50 mm Circle	T42	-0.985	0.479	0.923	-0.459	30.50	15.43	n/a
	T42a	-0.973	-0.281	0.817	0.199	26.91	7.14	n/a
	T42b	-0.995	0.020	0.956	-0.035	45.98	21.81	n/a
55x45 mm Egg	T42	-0.984	-0.292	0.951	0.302	30.89	10.57	1.801
	T42a	-0.969	-0.296	0.923	0.217	24.62	6.41	1.540
	T42b	-0.997	0.969	0.952	-0.956	44.90	25.24	0.973
45x30 mm Rectangle	T42	-0.768	-0.395	0.750	0.385	22.05	4.335	0.503
	T42a	-0.968	-0.234	0.926	0.088	44.79	4.28	1.299
	T42b	-0.970	-0.465	0.841	0.336	34.75	5.86	0.837
40 mm Square	T42	-0.883	-0.632	0.869	0.645	18.21	6.47	0.612
	T42a	-0.901	-0.685	0.818	0.813	13.66	4.81	0.368
	T42b	-0.995	0.988	0.818	-0.817	41.35	24.25	0.809
35 mm Square	T42	-0.598	-0.077	0.425	0.175	25.17	4.72	0.835
	T42a	-0.736	-0.759	0.739	0.750	19.23	4.27	0.562
	T42b	-0.989	-0.531	0.940	0.594	29.13	5.79	0.956

the design seemed to avoid over-constraining the tested objects. However, the lack of reconfiguration also resulted in a reduced reorientation workspace.

2) *Effect of Object Geometry*: Fig. 10 illustrates the effect of object geometry on the achievable workspace with the T42b hand. Motion in y is generally orthogonal to the free-swing trajectory of the fingers, so perhaps the radially-asymmetric objects' mobility were limited in that direction due to friction in the experimental setup. In particular, the overall xy workspace was most limited for the rectangular and square objects, which were often aligned against the hand palm or a finger link. The egg-shaped and circle geometries' curved surfaces made them easier to reconfigure within a grasp and avoid line contacts with the finger links or palm, made evident by the increased xy and reorientation workspaces. In the case of the egg-shaped objects, it should be noted that the evaluated workspace is dependent on the initial pose, and a different workspace could have been recorded if the object was initialized in a flipped configuration.

B. Workspace Analysis

One benefit of the experimental approach taken in this paper is the ability to examine correlation between actuator inputs and object coordinates, without needing a hand or hand-object Jacobian. Spearman's rho (r_s) was utilized to determine the degree of correlation between the actuator inputs (a_1 for the right-side finger and a_2 for the opposing left-side finger) and object pose components (x , y , and θ), as shown in Table II. An absolute value greater than 0.7 typically indicates a high degree of monotonic correlation. The nonlinear relation between object pose and actuator input makes Spearman's correlation more appropriate than the Pearson correlation for evaluation. A strong correlation identifies useful minimalist motion primitives, especially for cases where the object and/or hand model may be missing or inaccurate. These open-loop primitives could then be used in visual-servoing [29] or other model-free control

approaches, effectively employing the caging hand as a black box to make small relative adjustments to the object pose.

Table II reports low r_s values between the actuator inputs and object orientation for the radially-symmetric circular object, which is expected, as the caging hand's finger links cannot geometrically constrain the object orientation. This value generally improves for the other radially nonsymmetric objects, especially with the T42b design. However, the test manipulation of smaller objects, such as the 35-mm square and 45 × 30 mm rectangle, results in poor r_s values, especially with respect to orientation, even though they are radially nonsymmetric, since contact with the actuated finger links is not consistent or reliable. The opposing fingers do not interdigitate and consequently may collide and inhibit each other when manipulating objects much smaller than the hand's physical base separation.

The results report poor r_s between the actuator inputs and y for the T42 and T42a, though as Fig. 9 shows, this does not necessarily mean a lack of correlation or structure for the recorded y -coordinate values. In fact, Fig. 9 suggests that for certain subsets of the workspace data determined by bounds in x , the T42 and T42a tests would exhibit a Spearman correlation between the actuator values and y similar to those for the T42b. For more complex manipulators with additional actuators, it may be necessary to consider the Spearman correlation between the object pose parameters and functions of the actuator values, as opposed to considering each independently.

Despite having fewer degrees of freedom, recorded workspaces for the T42b design exhibited better r_s values than for the other hands, especially with respect to y . T42b's use of a one-link thumb in place of the two-link underactuated finger avoids inter-finger obstructions, and reduces the number of possible finger-object contacts, thereby avoiding over-constraint and jamming more effectively than the T42 and T42a. In contrast, the corresponding two-link fingers in the T42 and T42a tests can reconfigure in various ways for the same actuation

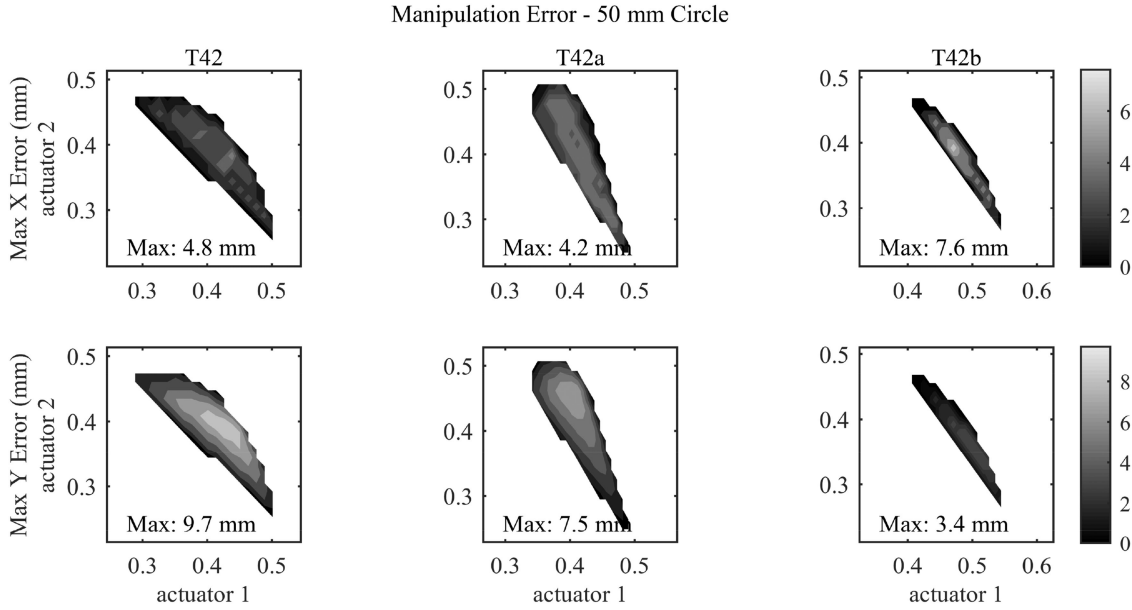


Fig. 11. Measure of repeatability with respect to the actuation space, evaluated for a 50-mm diameter circle and all three hand designs. Error is the range of object pose coordinates for a given set of actuation inputs. It is ideal to minimize the range of object poses for each unique actuation input.

tendon length constraint and may make contact with the object on either or both finger links. Qualitatively, we noticed repeated instances where a two-link underactuated finger would jam the object against the hand palm fully constraining the object and making the opposing finger ineffective.

Furthermore, the T42b tests consistently recorded a higher r_s for actuator 1 (driving the one-link thumb) than actuator 2 (driving the two-link underactuated finger) with respect to x , for all objects, and nearly all objects with respect to y . In previous work on mobile robotics, Brown and Jennings proposed a decoupled control scheme with dedicated “pusher” and “steerer” components [30], where the former produced the necessary force to maintain contact and move the object, and the latter guided the object motion by limiting its allowable free motion. A similar control philosophy could be used for caging manipulation, where the one-link thumb and two-link underactuated finger serves as the steerer and pusher, respectively. This leverages the adaptability of the two-link underactuated finger to efficiently maintain desirable caging conditions and the strong Spearman’s correlation between the one-link thumb and object coordinates to determine the final object pose.

C. Manipulation Error

As described in Section III, caging manipulation primitives can be executed for a range of initial object poses, invariant to contact state during the task, without ejecting the object, so we can experimentally evaluate the repeatability of the mapping between the actuator and object space. Due to the friction in the physical system, at both the contact locations and in the actuating tendon routing, operational error is expected relative to the expected energy minimal configuration.

With respect to the proposed energy field formulation, we can expect improved repeatability and minimal variance in pose

where the energy field gradients local to the energy minimal object configuration have the largest magnitude. A greater error can correspond to the subset of configurations where the object is caged but not securely grasped, or where system reconfigurations do not incur a significant change in system energy relative to nearby object poses in the object-contact space.

Fig. 11 shows the measured object pose error for a manipulated object with respect to the actuation workspace. The error is calculated by taking the range in measured object workspace coordinates for each unique actuation input. For the evaluated hand-object combinations, coordinate range was generally the greatest in the middle of the actuation workspace, corresponding to configurations where the object was constrained in the middle of the hand workspace. This is due to the objects having a secondary axis length smaller than the base separation between the two fingers, resulting in a larger free space for the object and increased mobility for the fingers to reconfigure in those configurations. Among the different hands, the T42b most consistently constrained the object’s y -coordinate value. Overall, the hands were generally more effective at reliably constraining the object in x -direction, matching the fingers’ typical motion trajectory.

D. Simulation Comparison

Fig. 6 shows experimental results collected from the methodology described in Section IV-D in the form of object start points (smaller symbols) and object end points (larger symbols) resulting from actuating the hand according to the actuation input pair, which are superimposed on each corresponding energy field. In each case, the hand-object system settled such that the object came to rest near the lowest energy position in the simulated energy field, regardless of the start position. The spread of end-points in the [0.4, 0.4] subplot is because the dual finger contact

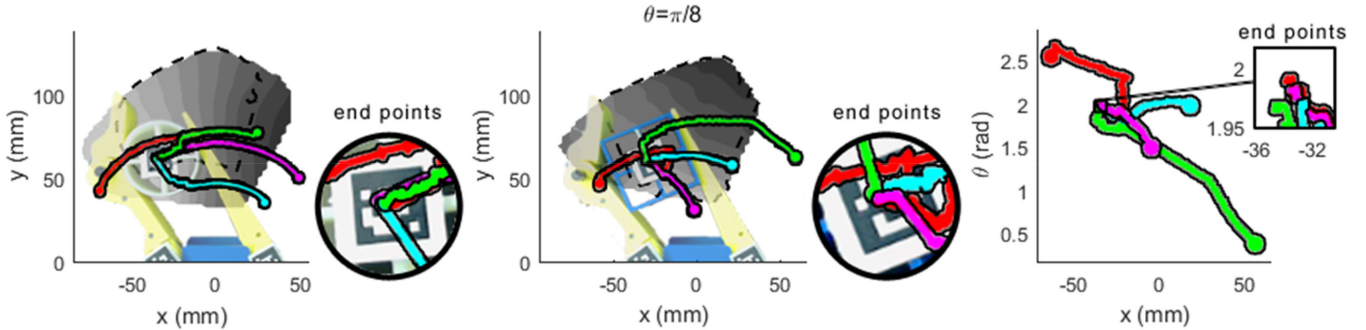


Fig. 12. Actuation input [0.4, 0.7] experimental trajectories from arbitrary selected start points. Left: Trajectories for 45-mm circle, superimposed over the corresponding energy map. Center: Trajectories for 45-mm square superimposed over the corresponding energy map. Right: Orientation trajectories for the 45-mm square object corresponding to the trajectories shown in the center panel.

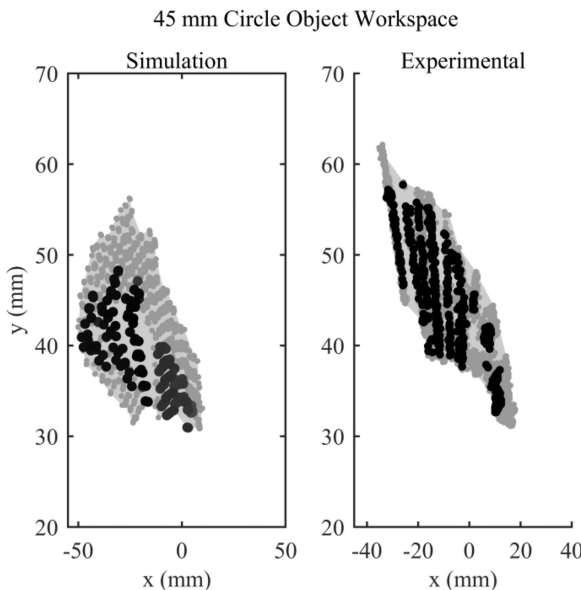


Fig. 13. For the simulation results, the gray points designate the lowest 1% of points, by energy value, from the energy fields corresponding to each sampled actuation input, and the black points designate the lowest 0.05% of points. In the experimental results, the black points designate positions where the object came to rest (low energy positions), and the gray points are positions captured during motion.

is never established with this actuation input pair (no dashed lines).

Fig. 12 shows experimentally collected object manipulation trajectories superimposed on corresponding simulated actuator energy maps. For a given actuation input, all object trajectories terminate in nearly the same position, and orientation in the case of the square object, regardless of the starting position. This position is in a low-energy region of the simulated actuator energy workspace. Additionally, object trajectories roughly follow the gradients of the energy maps, as predicted.

Fig. 13 compares the object workspaces approximated from the methodology detailed in Section IV with experimental results for the T42b. The simulated model uses zero-thickness finger links, so a padding equivalent to the thickness of the fingers used in the experimental platform was added to the object

geometry. Each actuator was sampled at 0.05 intervals between inputs 0.1 and 1.0 (normalized to the max travel of the actuator), inclusive, so the simulated model considered 361 generated object energy fields for the T42b. For each energy field, only the points for which both actuators in the system are doing non-negative work are considered, and when sorted by energy value, the lowest 1% from each energy field were initially extracted as candidate object workspace configurations (shown in gray in Fig. 13). Between the initial and final configurations of a caging manipulation primitive, the grasp quality in terms of the forces applied to the object may vary considerably.

In practice, to avoid overheating the servos, actuator reference commands are limited by the object geometry, and at the same time, loose grasps where the fingers barely make contact with the object are avoided with the implementation of the squeezing command described in Section IV-C. The analysis excludes actuation commands matching these undesirable conditions by only considering cases where 20 to 80% of the contact space has a positive energy value. The authors acknowledge that the selection criteria for the final simulated grasp poses rely on arbitrary threshold values that will be further investigated in the future work.

The results for the 45-mm circle object, detailed in Fig. 13, are encouraging, as the union of the bottom 1% of energy field points appears to provide a reasonable approximation for the expected object motion during caging manipulation. Simulation errors could be due to insufficient joint discretization in the formulation of the theoretical hand workspace. To make the problem computationally tractable, the system joint values were sampled at 0.05 rad (2.86 deg) intervals. Experimental errors are most likely due to friction and jamming at contact, despite the use of low-friction ABS surfaces in both the hand and object.

Note that this model does not directly address friction at contact. Although researchers have assumed frictionless contacts or “slippery” objects, even in the analysis of both point-based and linkage-based caging [31], [32], it remains a challenging and unavoidable aspect of physical manipulation tasks. Some researchers have proposed the use of “active surfaces” to directly modulate sliding at contact as a potential solution [33].

It is possible that the gradient local to the energy minimal configuration in the object energy fields produced in this analysis can be used to approximate the magnitude of frictional forces that each motion primitive can overcome, but that was beyond the scope of this initial effort. In addition, direct manipulation moves with enveloping grasps rely on a considerable degree of sliding between the object and actuated components, and controlled, repeatable sliding motions have been difficult to reliably model even in well-structured simple systems where the material and geometric properties are known *a priori*.

VI. GAITING AND REGRASPING

The caging manipulation strategy allows for intermittent losses of contact that can help mitigate issues with friction and jamming. Formally, finger-gaiting and regrasping have been proposed as strategies to recycle or reset the workspace of the finger and/or other actuated components [1]. Traditionally, both approaches can have strict requirements, as finger-gaiting requires a redundant set of fingers that can facilitate the disengagement and reengagement of a finger required for a stable grasp, and regrasping necessitates the ability to robustly release the object in the environment to attempt a new grasp. Mechanical hardware may not be sufficient to enable the former, and the task requirements may not permit the latter. The caging attribute of the proposed manipulation primitives offers a hybrid solution.

Caging enables limited object mobility, but to a sufficient degree for some subset of contacts to be completely disengaged. Simultaneously, the object is technically released, albeit confined to a subset of the operational environment still bounded by the hand components (C_{cage}). Again, consider the case of the human-hand picking up an object sub-optimally and then fumbling it within the hand into a more optimal grasp. The contact states are unlikely to stay well-structured, and the grasp may loosen at various stages to help overcome friction and jamming, or allow the object some mobility mid-realignment.

This extension of the caging manipulation primitives was evaluated by modifying the servo trajectory between commanded motions, as shown in Fig. 14. Instead of moving to the desired servo positions directly, the direct move is discretized into steps, and the two fingers alternate active motions. Qualitatively, this jostles the object within the grasp, as each finger perturbs the object in a nonprehensile manner.

Fig. 15 shows an example of the object workspaces evaluated for direct and gaited actuator motion profiles. Despite the use of ABS in both the object and fingerpad surfaces in the experimental setup, friction was not negligible, thereby limiting the reachable workspace size. As contact is disengaged more frequently through gaiting, the dissipative effects from friction restrict the object motion less, and the hand can achieve a larger object workspace, in terms of both the final grasped object poses (black points) and the intermediate object poses during the execution of the manipulation primitive (grey region). Despite the uncoordinated breaks in contact, the object remained

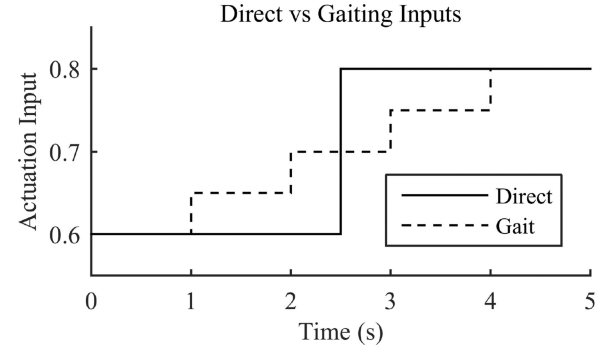


Fig. 14. Summary of the difference in actuator inputs for a direct versus a gaited motion.

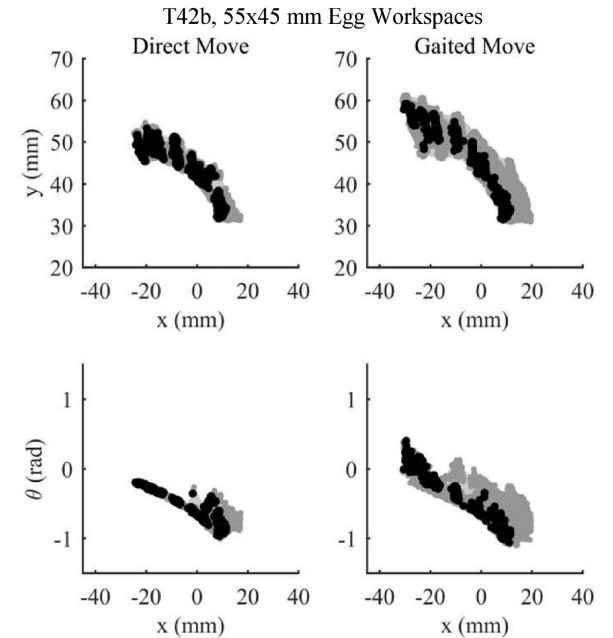


Fig. 15. Comparison between the workspaces evaluated through direct actuator move commands versus gaited actuator move commands.

constrained to the hand workspace, albeit only demonstrated here for the simplified planar case.

Table III provides more details in comparing gaiting and direct motion profiles. It is most notable that gaiting improved the Spearman's correlation between the object y -coordinate and both actuator inputs. Object motion in the y -direction, which is generally orthogonal to the finger free-swing trajectory in these planar hands, would be most limited by the friction at contact. These workspace characteristics suggest that a repeated and properly bounded release-and-regrasp gait can help us to compensate for the effects of friction due to unknown material properties. The media attachment to this paper further demonstrates some practical spatial applications of caging, where instead of relying on explicitly controlled contact vectors, a series of gaited caging motions are made, causing the manipulated object to settle into the most stable grasping configuration.

TABLE III
T42B CAGING MANIPULATION EVALUATION—GAITING

Object	Actuation	$r_s(a_1, x)$	$r_s(a_1, y)$	$r_s(a_2, x)$	$r_s(a_2, y)$	$range(x)$	$range(y)$
		(mm)	(mm)				
45 mm Circle	Direct	-0.993	0.927	0.958	-0.921	44.82	24.53
	Gaited	-0.986	0.965	0.928	-0.952	48.22	27.32
55x45 mm Egg	Direct	-0.973	0.944	0.913	-0.954	35.65	21.50
	Gaited	-0.960	0.960	0.872	-0.977	42.14	27.73

VII. CONCLUSION

In this paper, we analyzed *whole-hand caging manipulation*, a manipulation primitive, which could be also be described as in-hand fumbling or shuffling. This primitive was modeled as an extension of the caging problem, with an energy state assigned to each corresponding configuration according to the commanded actuation inputs. The resulting energy field and associated gradients provided insight into the expected object trajectory and grasp stability. The caging characteristic allowed for open-loop trajectories that avoid object ejection or loss of grasp without detailed knowledge of the contact conditions. A methodology to efficiently approximating the energy field workspace for a given object geometry was detailed, and several examples for different hand topologies were demonstrated. In addition, this manipulation primitive was evaluated on a physical test setup for an extended set of object geometries and planar underactuated hand designs.

Although the proposed manipulation primitive and accompanying model relied on several assumptions that were unrealistic in practice (e.g., frictionless contacts), as long as sufficient bounds on the object workspace could be maintained such that the object was not lost, the hand could continue to manipulate the object toward the desired pose, especially when coupled with visual or other feedback. Examples of open-loop gaiting motions, made possible by caging, were also demonstrated as a means of extending the manipulation workspace and compensating for different coefficients of friction. This might run counter to past traditional approaches to dexterous manipulation, which require object stability and well-maintained contact conditions within the grasp at all instances of the executed task.

The presented methodology can be applied to spatial caging scenarios as well, but as other researchers have stated [10], [11], the increased dimensionality may make a thorough computation infeasible. However, as Section V detailed, energy fields may only need to be computed for classes of objects with similar geometry, not necessarily each unique object geometry. Also, a sparse or variable workspace discretization may provide sufficient analysis of the expected object behavior.

While the proposed caging manipulation primitive can be applied on any hand design, it is particularly useful in underactuated hands, which are typically designed to passively cage around the object, regardless of the particularities of its geometry. Caging manipulation extends the underactuated hand's passive adaptation and applies a bias to the object, constrained to its allowable workspace relative to the hand. We hope that

the robustness demonstrated by the experimental examples will encourage researchers to consider other manipulation primitives that relax grasp constraints where possible, enabling useful manipulation without the burden or added practical complexity of maintaining fixed contacts.

REFERENCES

- [1] A. Bicchi, “Hands for dexterous manipulation and robust grasping: A difficult road toward simplicity,” *IEEE Trans. Robot. Autom.*, vol. 16, no. 6, pp. 652–662, Dec. 2000.
- [2] Z. Li, P. Hsu, and S. Sastry, “Grasping and coordinated manipulation by a multifingered robot hand,” *Int. J. Robot. Res.*, vol. 8, no. 4, pp. 33–50, 1989.
- [3] M. T. Mason and J. K. Salisbury, *Robot Hands and the Mechanics of Manipulation*. Cambridge, MA, USA: MIT Press, 1985.
- [4] M. Grebenstein *et al.*, “The hand of the DLR hand arm system: Designed for interaction,” *Int. J. Robot. Res.*, vol. 31, no. 13, pp. 1531–1555, Nov. 2012.
- [5] T. Senoo, Y. Yamakawa, S. Mizusawa, A. Namiki, M. Ishikawa, and M. Shimojo, “Skillful manipulation based on high-speed sensory-motor fusion,” in *Proc. Int. Conf. Robot. Automat.*, 2009, pp. 1611–1612.
- [6] G. Vassura and A. Bicchi, “Whole-hand manipulation: Design of an articulated hand exploiting all its parts to increase dexterity,” in *Robots and Biological Systems: Towards a New Bionics?*. New York, NY, USA: Springer, 1993, pp. 165–177.
- [7] L. U. Odhner, R. R. Ma, and A. M. Dollar, “Open-loop precision grasping with underactuated hands inspired by a human manipulation strategy,” *IEEE Trans. Robot.*, vol. 10, no. 3, pp. 625–33, Jul. 2013.
- [8] M. N. Ahmadabadi and E. Nakano, “A ‘constrain and move’ approach to distributed object manipulation,” *IEEE Trans. Robot. Autom.*, vol. 17, no. 2, pp. 157–172, Apr. 2001.
- [9] W. Wan, R. Fukui, M. Shimosaka, T. Sato, and Y. Kuniyoshi, “Grasping by caging: A promising tool to deal with uncertainty,” in *Proc. Int. Conf. Robot. Automat.*, 2012, pp. 5142–5149.
- [10] S. Makita and Y. Maeda, “3-D multifingered caging: Basic formulation and planning,” in *Proc. Int. Conf. Intell. Robot. Syst.*, 2008, pp. 2697–2702.
- [11] R. Diankov, S. S. Srinivasa, D. Ferguson, and J. Kuffner, “Manipulation planning with caging grasps,” in *Proc. IEEE-RAS Int. Conf. Humanoid Robot.*, 2008, pp. 285–292.
- [12] A. Rodriguez, M. T. Mason, and S. Ferry, “From caging to grasping,” *Int. J. Robot. Res.*, vol. 31, no. 7, pp. 886–900, Apr. 2012.
- [13] A. Rodriguez, M. T. Mason, and S. S. Srinivasa, “Manipulation capabilities with simple hands,” in *Experimental Robotics*. New York, NY, USA: Springer, 2014, pp. 285–299.
- [14] L. U. Odhner *et al.*, “A compliant, underactuated hand for robust manipulation,” *Int. J. Robot. Res.*, vol. 33, no. 5, pp. 736–752, 2014.
- [15] L. U. Odhner and A. M. Dollar, “Dexterous manipulation with underactuated elastic hands,” in *Proc. Int. Conf. Robot. Automat.*, 2011, pp. 5254–5260.
- [16] A. Sudsang, J. Ponce, and N. Srinivasa, “Algorithms for constructing immobilizing fixtures and grasps of three-dimensional objects,” *Algorithmic Foundations of Robotics II*, Natick, MA: Peters, 1997, pp. 363–380.
- [17] G. A. Kragten and J. L. Herder, “The ability of underactuated hands to grasp and hold objects,” *Mech. Mach. Theory*, vol. 45, no. 3, pp. 408–425, 2010.
- [18] D. M. Aukes *et al.*, “Design and testing of a selectively compliant underactuated hand,” *Int. J. Robot. Res.*, vol. 33, pp. 721–735, Apr. 2014.

- [19] Y. Maeda and T. Asamura, "Sensorless in-hand caging manipulation," in *Proc. Int. Conf. Intell. Auton. Syst.*, 2016, pp. 255–267.
- [20] Y. Maeda, T. Asamura, T. Egawa, and Y. Kurata, "Geometry-based manipulation through robotic caging," in *Proc. IEEE/RSJ IROS 2014 Workshop Robot Manipulation*, 2014.
- [21] R. R. Ma and A. M. Dollar, "Linkage-based analysis and optimization of an underactuated planar manipulator for in-hand manipulation," *J. Mech. Robot.*, vol. 6, no. 1, 2014, Art. no. 011002.
- [22] I. Kao and M. R. Cutkosky, "Quasistatic manipulation with compliance and sliding," *Int. J. Robot. Res.*, vol. 11, no. 1, pp. 20–40, Feb. 1992.
- [23] J. Mahler, F. T. Pokorny, Z. McCarthy, A. F. Van Der Stappen, and K. Goldberg, "Energy-bounded caging: Formal definition and 2-D energy lower bound algorithm based on weighted alpha shapes," *IEEE Robot. Autom. Lett.*, vol. 1, no. 1, pp. 508–515, Jan. 2016.
- [24] B. S. Baker, E. Grossé, and M. H. Nj, "Stable prehension with three fingers," in *Proc. Symp. Theory Comput.*, 1985, pp. 114–120.
- [25] T. Yamada, T. Koishikura, Y. Mizuno, N. Mimura, and Y. Funahashi, "Stability analysis of 3-D grasps by a multifingered hand," in *Proc. Int. Conf. Robot. Automat.*, 2001, pp. 2466–2473.
- [26] S. Garrido-Jurado, R. Munoz-Salinas, F. J. Madrid-Cuevas, and M. J. Marin-Jimenez, "Automatic generation and detection of highly reliable fiducial markers under occlusion," *Pattern Recognit.*, vol. 47, no. 6, pp. 2280–2292, 2014.
- [27] L. U. Odhner, R. R. Ma, and A. M. Dollar, "Exploring dexterous manipulation workspaces with the iHY hand," *J. Robot. Soc. Jpn.*, vol. 32, no. 4, pp. 318–322, 2014.
- [28] R. B. Rusu and S. Cousins, "3-D is here: Point cloud library (PCL)," in *Proc. Int. Conf. Robot. Automat.*, 2011, pp. 1–4.
- [29] B. Calli and A. M. Dollar, "Vision-based precision manipulation with underactuated hands: Simple and effective solutions for dexterity," in *Proc. Int. Conf. Intell. Robot. Syst.*, 2016, pp. 1012–1018.
- [30] R. G. Brown and J. S. Jennings, "A pusher/steerer model for strongly cooperative mobile robot manipulation," in *Proc. Int. Conf. Intell. Robot. Syst.*, 1995, pp. 562–568.
- [31] J. C. Trinkle, R. C. Ram, A. O. Farahat, and P. F. Stiller, "Dexterous manipulation planning and execution of an enveloped slippery workpiece," in *Proc. Int. Conf. Robot. Automat.*, 1993, pp. 442–448.
- [32] T. Yamawaki and M. Yashima, "Randomized planning and control strategy for whole-arm manipulation of a slippery polygonal object," in *Proc. IEEE/RSJ Int. Conf. Intell. Robot. Syst.*, 2013, pp. 2485–2492.
- [33] R. Krug *et al.*, "Velvet fingers: Grasp planning and execution for an underactuated gripper with active surfaces," in *Proc. Int. Conf. Robot. Automat.*, 2014, pp. 3669–3675.
- [34] M. Raymond R. W. G. Bircher, and A. M. Dollar, "Toward robust, whole-hand caging manipulation with underactuated hands," in *Proc. Int. Conf. Robot. Automat.*, 2017, pp. 1336–1342.
- [35] J. Mahler, F. T. Pokorny, S. Niyaz, and K. Goldberg, "Synthesis of energy-bounded planar caging grasps using persistent homology," *IEEE Trans. Automat. Sci. Eng.*, vol. 15, no. 3, pp. 908–918, Jul. 2018.
- [36] W. Wan, F. Lu, and R. Fukui, "Error-tolerant manipulation by caging," *Signal Process.*, vol. 120, pp. 721–730, 2016.
- [37] C. Eppner and O. Brock, "Planning grasp strategies that exploit environmental constraints," in *Proc. Int. Conf. Robot. Automat.*, 2015, pp. 4947–4952.
- [38] H. A. Bunis, E. D. Rimon, T. Golan, and A. Shapiro, "Caging polygonal objects using equilateral three-finger hands," *IEEE Robot. Automat. Lett.*, vol. 2, no. 3, pp. 1672–1679, Jan. 2017.
- [39] T. F. Allen, E. D. Rimon, and J. W. Burdick, "Two-finger caging of 3-D polyhedra using contact space search," in *Proc. Int. Conf. Robot. Automat.*, 2014, pp. 2005–2012.



Raymond R. Ma (S'11) received the B.S. degrees in mechanical engineering and computer science from Massachusetts Institute of Technology, Cambridge, MA, USA, in 2010, and the M.S. and Ph.D. degrees in mechanical engineering from Yale University, New Haven, CT, USA, in 2013 and 2016, respectively.

He is currently an Engineer with the NASA Jet Propulsion Laboratory, Pasadena, CA, USA.



Walter G. Bircher (S'16) received the B.S. degree in mechanical engineering in 2014, from the University of Nebraska-Lincoln, Lincoln, NE, USA, and the M.S. degree in mechanical engineering in 2018, from Yale University, New Haven, CT, USA, where he is currently working toward the Ph.D. degree in engineering.

His research focuses on the dexterous capabilities of compliant underactuated robotic grippers.



Aaron M. Dollar (SM'06) received the B.S. degree in mechanical engineering from University of Massachusetts at Amherst, Amherst, MA, USA, in 2000, and the S.M. and Ph.D. degrees in engineering sciences from Harvard University, Cambridge, MA, in 2002 and 2007, respectively.

He is the John J. Lee Assistant Professor of mechanical engineering and materials science with Yale University, New Haven, CT, USA. He is the Editor and Cofounder of RoboticsCourseWare.org, an open repository for robotics pedagogical materials. His research interests include robotic grasping and manipulation, tactile sensing, prosthetics and rehabilitation robotics, and robot locomotion.

Prof. Dollar is an active member of the American Society of Mechanical Engineers and the American Society of Engineering Education.